Supplementary information

Self-activated ultrahigh chemosensitivity of oxide thin film nanostructures for transparent sensors

Hi Gyu Moon[1,2], Young-Soek Shim[1], Do Hong Kim[1], Hu Young Jeong[3], Myoungho Jeong[4], Joo Young Jung[5], Seung Min Han[5], Jong-Kyu Kim[6], Jin-Sang Kim[1], Hyung-Ho Park[2], Jong-Heun Lee[7], Harry L. Tuller[8], Seok-Jin Yoon[1]* & Ho Won Jang[9]*

[1]Electronic Materials Research Center, Korea Institute of Science and Technology, Seoul 136-791, Republic of Korea

[2]Department of Materials Science and Engineering, Yonsei University, Seoul 120-749, Republic of Korea

[3]UNIST Central Research Facilities, Ulsan National Institute of Science and Technology, Ulsan 689-798, Republic of Korea

[4]Department of Materials Science and Engineering, Korea Advanced Institute of Science and Technology, Daejeon 305-701, Republic of Korea

[5]Graduate School of Energy Environment Water Sustainability, Korea Advanced Institute of Science and Technology, Daejeon 305-701, Republic of Korea

[6]Department of Materials Science and Engineering, Pohang Institute of Science and Technology, Pohang 790-784, Republic of Korea

[7]Department of Materials Science and Engineering, Korea University, Seoul 136-713, Republic of Korea

[8]Department of Materials Science and Engineering, Massachusetts Institute of Technology, Cambridge, Massachusetts 02139, USA

[9]Department of Materials Science and Engineering, Research Institute of Advanced Materials, Seoul National University, Seoul 151-742, Republic of Korea

*e-mail: hwjang@snu.ac.kr; sjyoon@kist.re.kr

Supplementary Table S1. Ambient air quality standard (AAQS) levels of European Union (EU), United States (US) and Korea for CO, NO_2, SO_2 pollutants which are considered harmful to public health and the environment. More detailed information about the AAQS levels is available on http://www.airkorea.or.kr and http://www.epa.gov/air/airpollutants.html.

Pollutant	Averaging time	Level		
		EU	US	Korea
NO_2	1 year	21 ppb	53 ppb	30 ppb
SO_2	1 hours	130 ppb	75 ppb	150 ppb
CO	8 hours	8.6 ppm	9 ppm	8.6 ppm

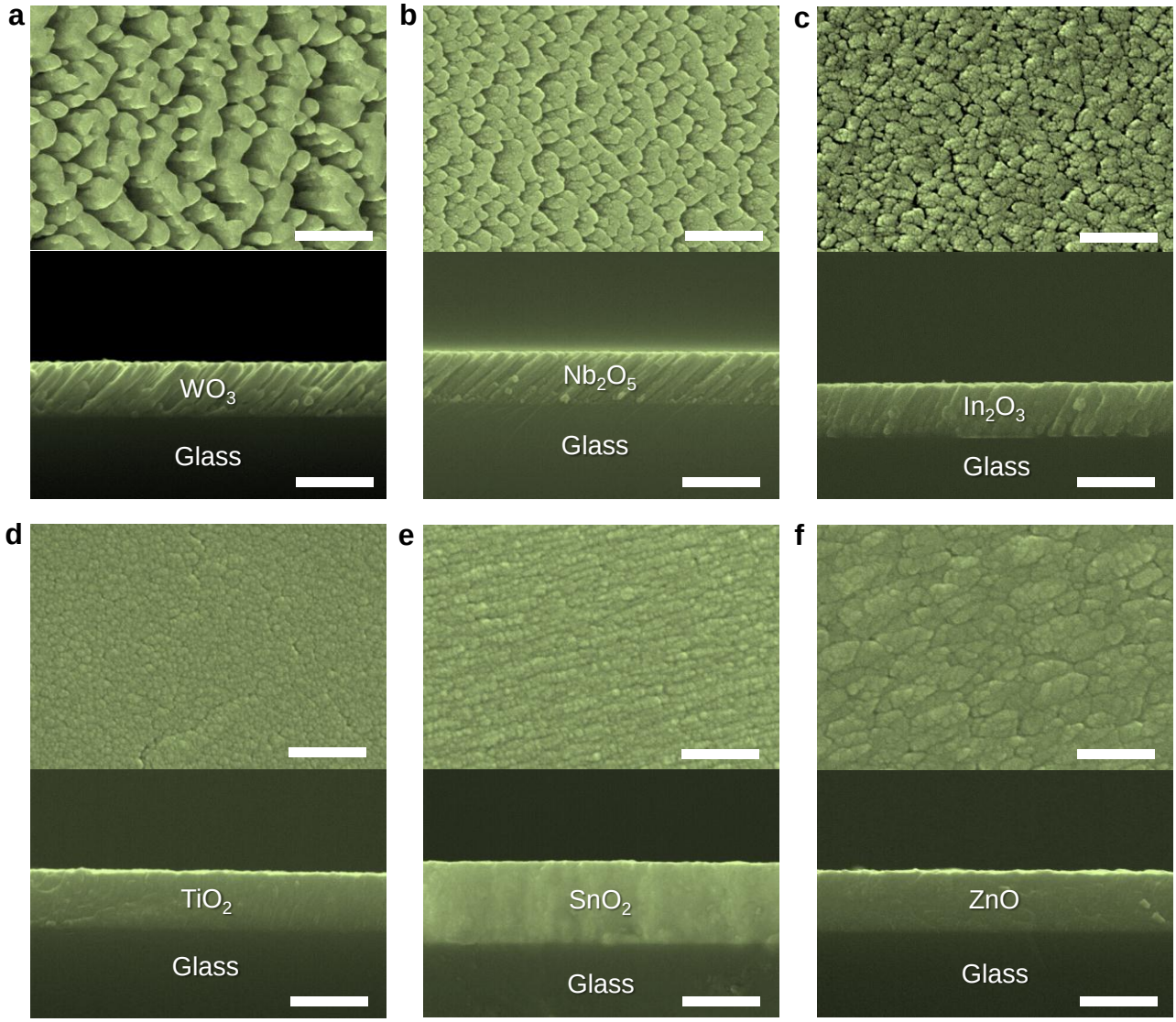

Supplementary Figure S1 | Various metal oxide thin films by GAD. a–f, Cross-sectional and plain-view and cross-sectional SEM images of WO_3 (**a**), Nb_2O_5 (**b**), In_2O_3 (**c**), TiO_2 (**d**), SnO_2 (**e**), and ZnO (**f**) thin films. Scale bar, 600 nm.

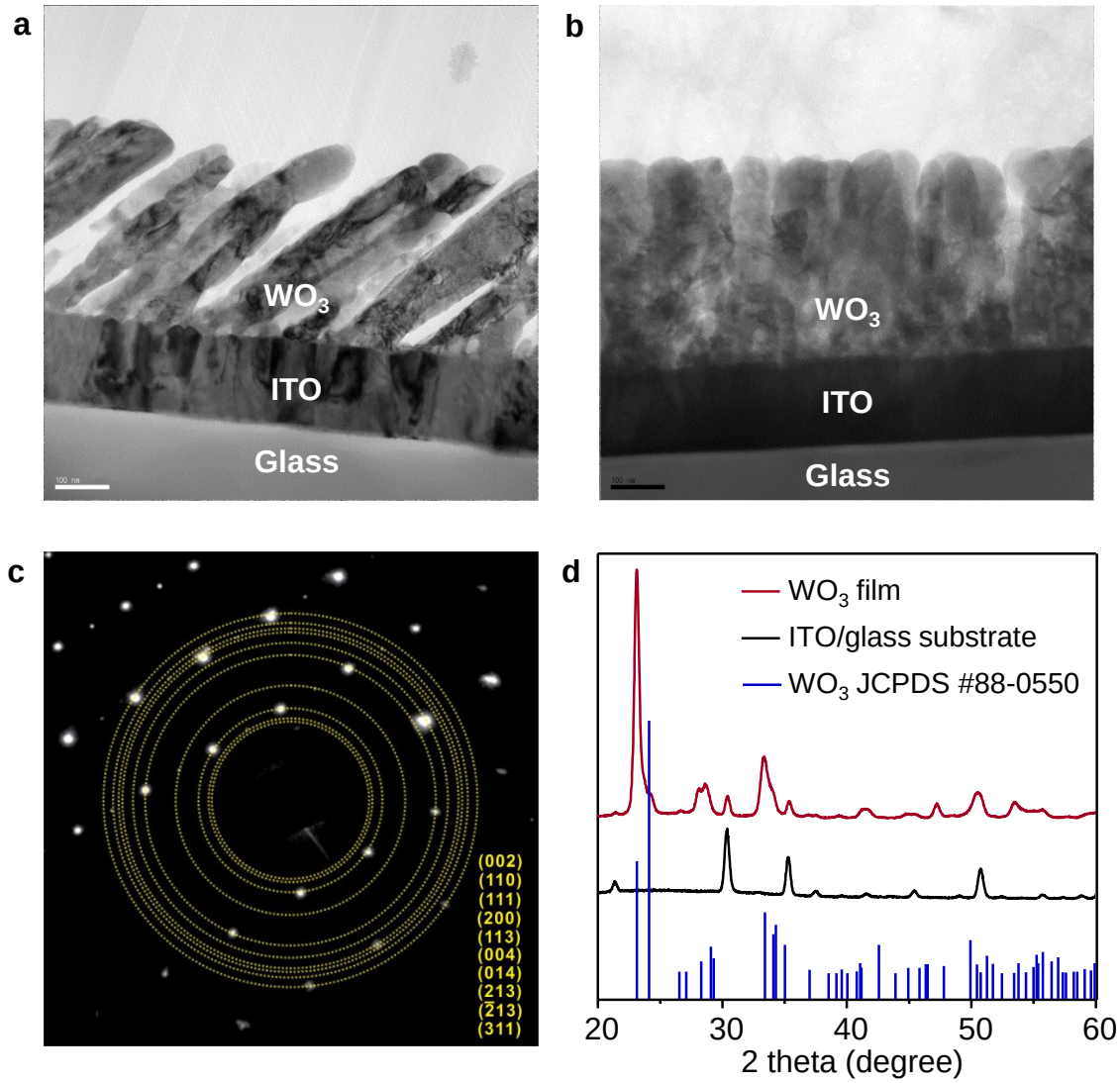

Supplementary Figure S2 | Structural characterizations of nanocolumar WO_3 films. **a,b,** Cross-sectional TEM images of nanocolumnar WO_3 film on ITO electrodes cut along (**a**) and cross (**b**) the ITO IDEs. Scale bar, 100 nm. **c,** Selected area diffraction pattern from TEM for the nanocolumnar WO_3 film. The dot-lined circles corresponds to *d*-spacings of the monoclinic WO_3 phase with lattice parameters of a = 5.261 Å, b = 5.128 Å, c = 7.650 Å and β = 92.050^{o}. **d,** Glancing angle X-ray diffraction patterns of a bare ITO/glass substrate and of a nanocolumnar WO_3 film on the substrate. The reflections of the monoclinic phase of WO_3 (JCPDS # 88-0550) are presented with blue lines.

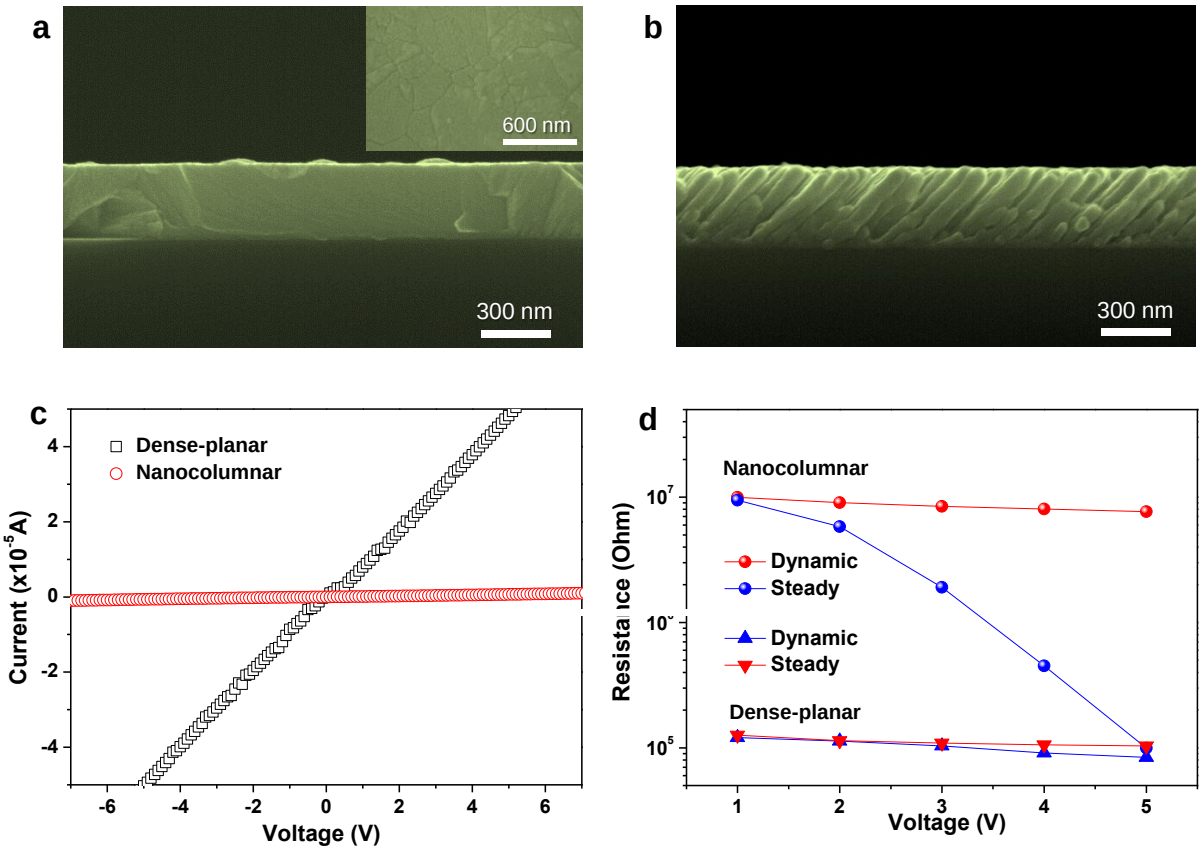

Supplementary Figure S3 | Morphological and electrical properties of dense-planar and nanocolumnar WO_3 thin film sensors. a,b Cross-sectional SEM image of the WO_3 sensing films of the plain WO_3 thin film sensor (**a**) and the nanocolumnar WO_3 thin film sensor (**b**). Insets: Plain-view SEM images. **c,** Current-voltage (*I-V*) characteristics of the dense-planar and nanocolumnar WO_3 thin film sensors. **d,** Resistances of the sensors as a function of the applied bias voltage. Dynamic resistances were evaluated from the I-V curves in **c**. Steady resistances were measured 10 min later after applying the bias voltage. The large difference between dynamic and steady resistances for the nanocolumnar sensor indicates self-heating in the sensing film.

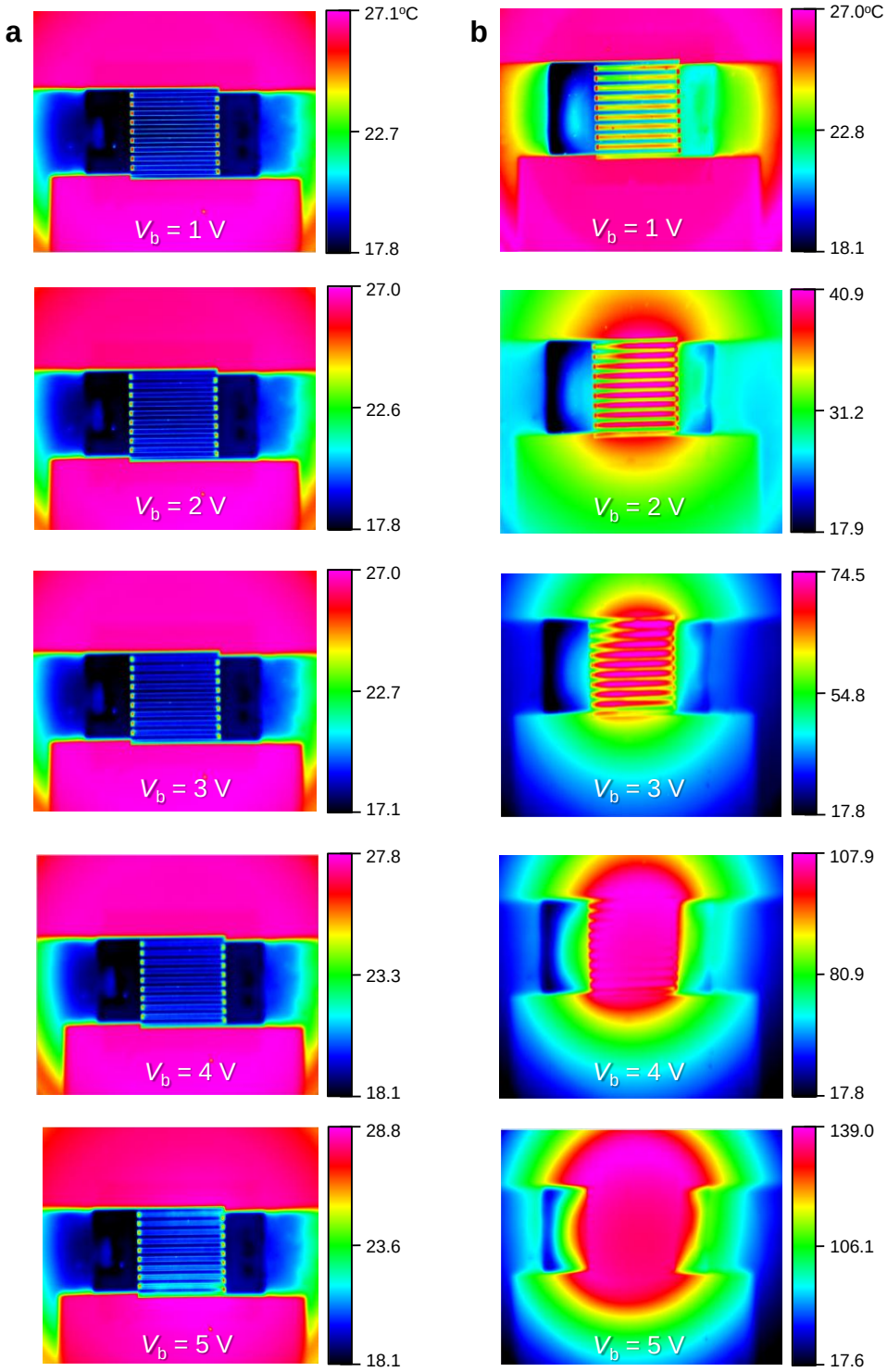

Supplementary Figure S4 | Self-activation in sensors. a,b, Thermographic images of the plain WO_3 thin film sensor (**a**) and the nanocolumnar WO_3 thin film sensor (**b**) as a function of the applied bias voltage (V_b).

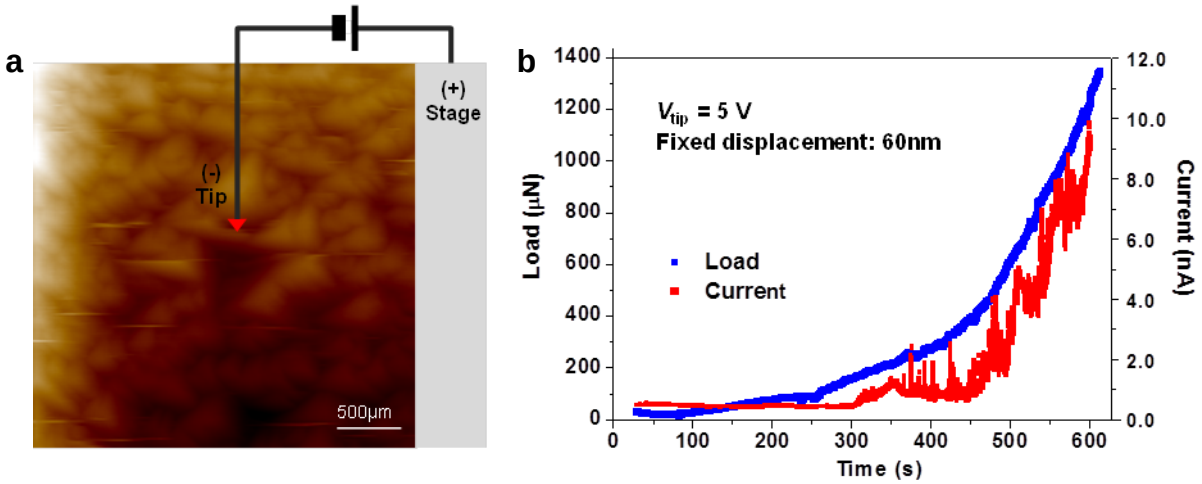

Supplementary Figure S5 | Nano ECR measurements of the nanocolumnar WO_3 thin film sensor. a, SPM(Scanning Probe Microscope) image showing location of measurement on the clustered nanocolumns. **b,** Force and current as a function of time at a fixed displacement of 60nm. The increase of force and current with time at the tip implies the thermal expansion of the nanocolumnar film due to joule heating.

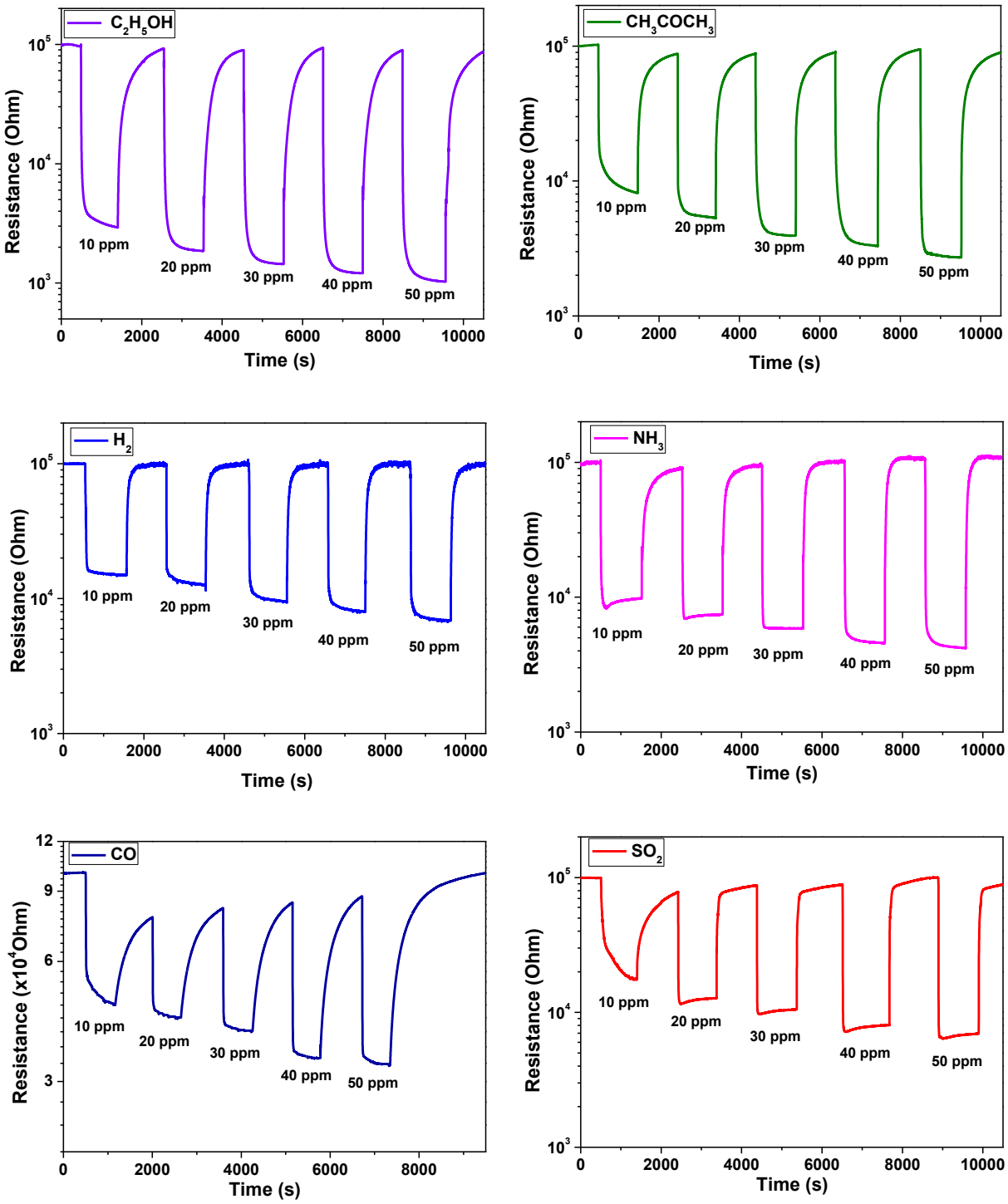

Supplementary Figure S6 | Responses of the nanocolumnar WO_3 thin film sensor to various gases. The measurements were carried out without external heating at the applied bias voltage of 5 V. Sensor shows linear change in response with varying concentration of test gas,.

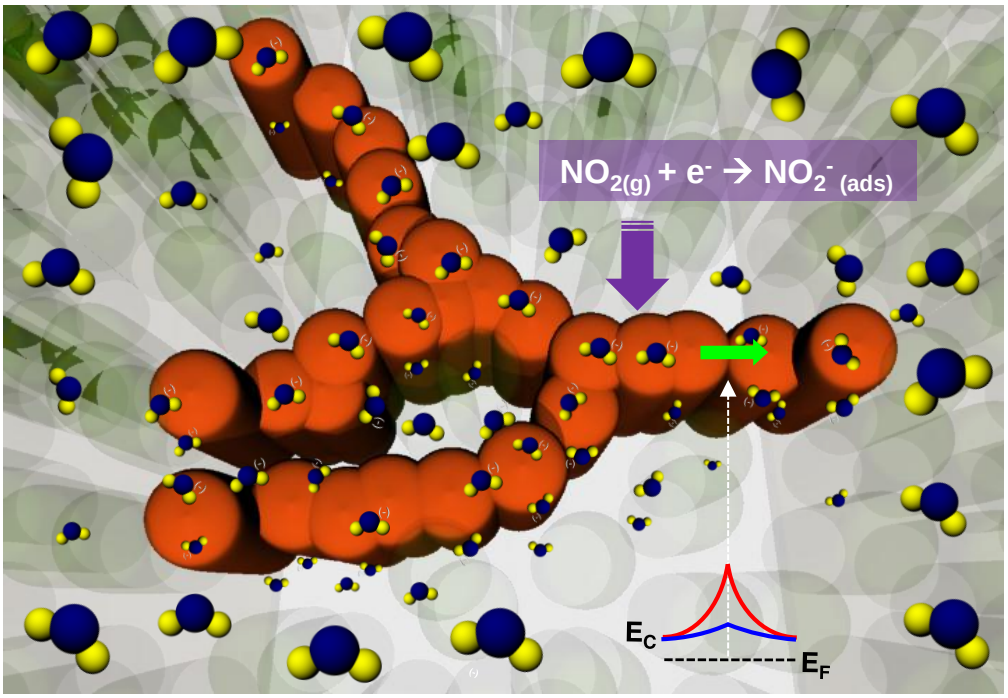

Supplementary Figure S7 | Schematic illustration of the NO_2 sensing mechanism of the nanocolumnar WO_3 thin film sensor. The gas molecules easily access the active nanocolumns, which act as current pathways, and remains hot due to self-heating. At the narrow neck, a high potential barrier for current flow is formed. The green arrow indicates current flow. The lower conduction band edges (blue lines) correspond to the potential barrier in air and the upper conduction band edges (red lines) correspond to the barrier that arises from exposure to NO_2.

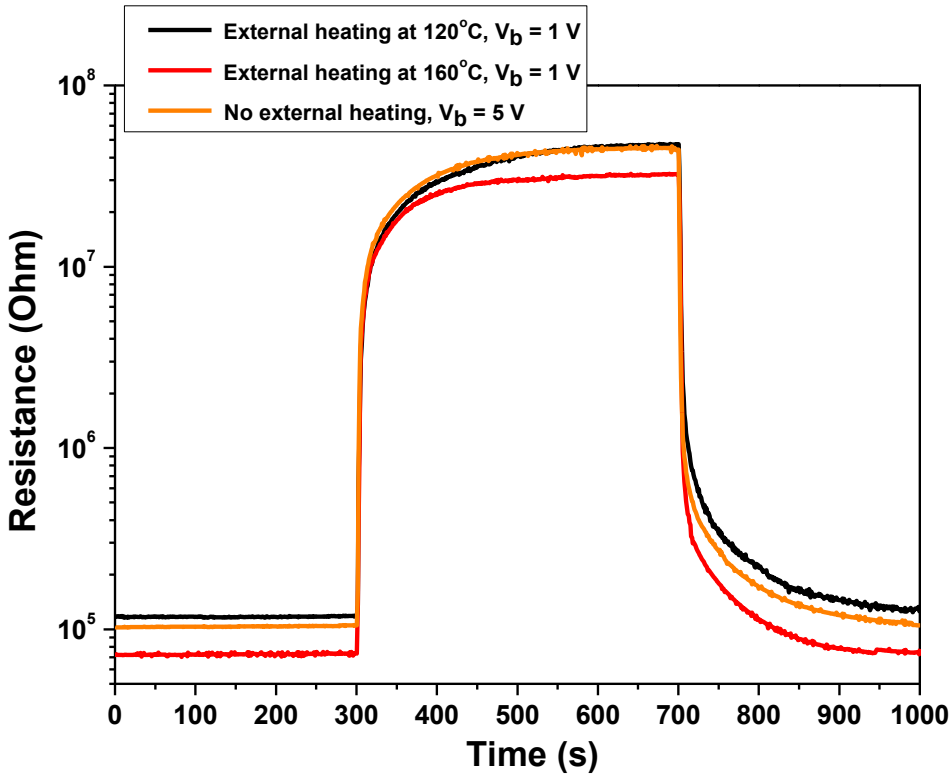

Supplementary Figure S8 | Comparison of the response of the nanocolumnar WO_3 thin film sensor to 5 ppm NO_2 with and without external heating. For measurements with external heating, an applied bias voltage of 1 V was used to minimize self-heating in the film.

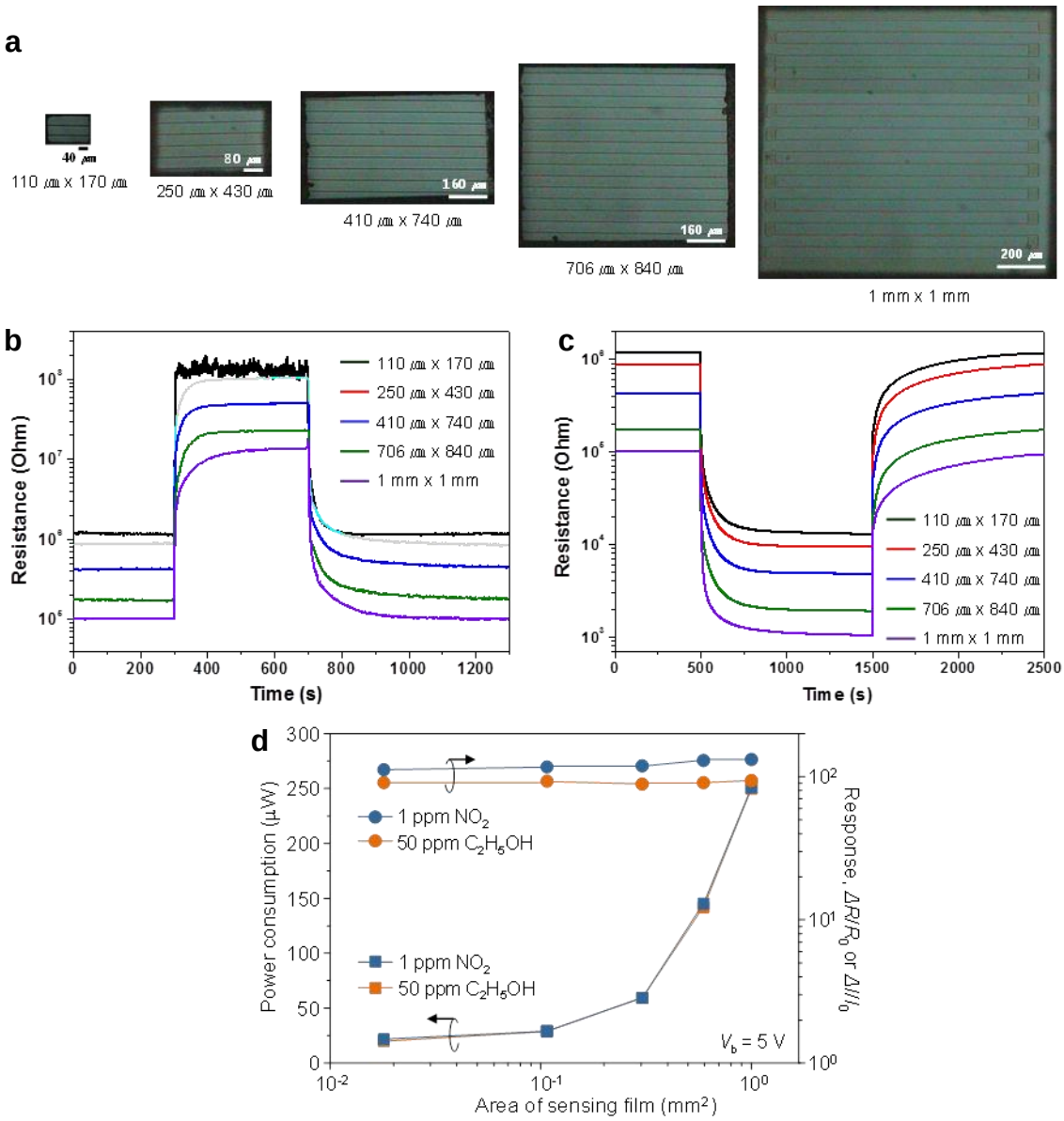

Supplementary Figure S9 | Dependence of sensor response and power consumption on the area of the sensing film. a, Optical microscopy images of 5 different areas of nanocolumnar WO_3 thin film sensors. **b,c,** Sensing transients of the nanocolumnar WO_3 thin film sensors with different sensing area to 1 ppm NO_2 (**b**) and 50 ppm ethanol (**c**). The applied bias voltage to the sensors was 5 V. **d,** Power consumption and response of nanocolumnar WO_3 thin film sensors to 1 ppm NO_2 and 50 ppm C_2H_5OH as a function of the area of the sensing film.

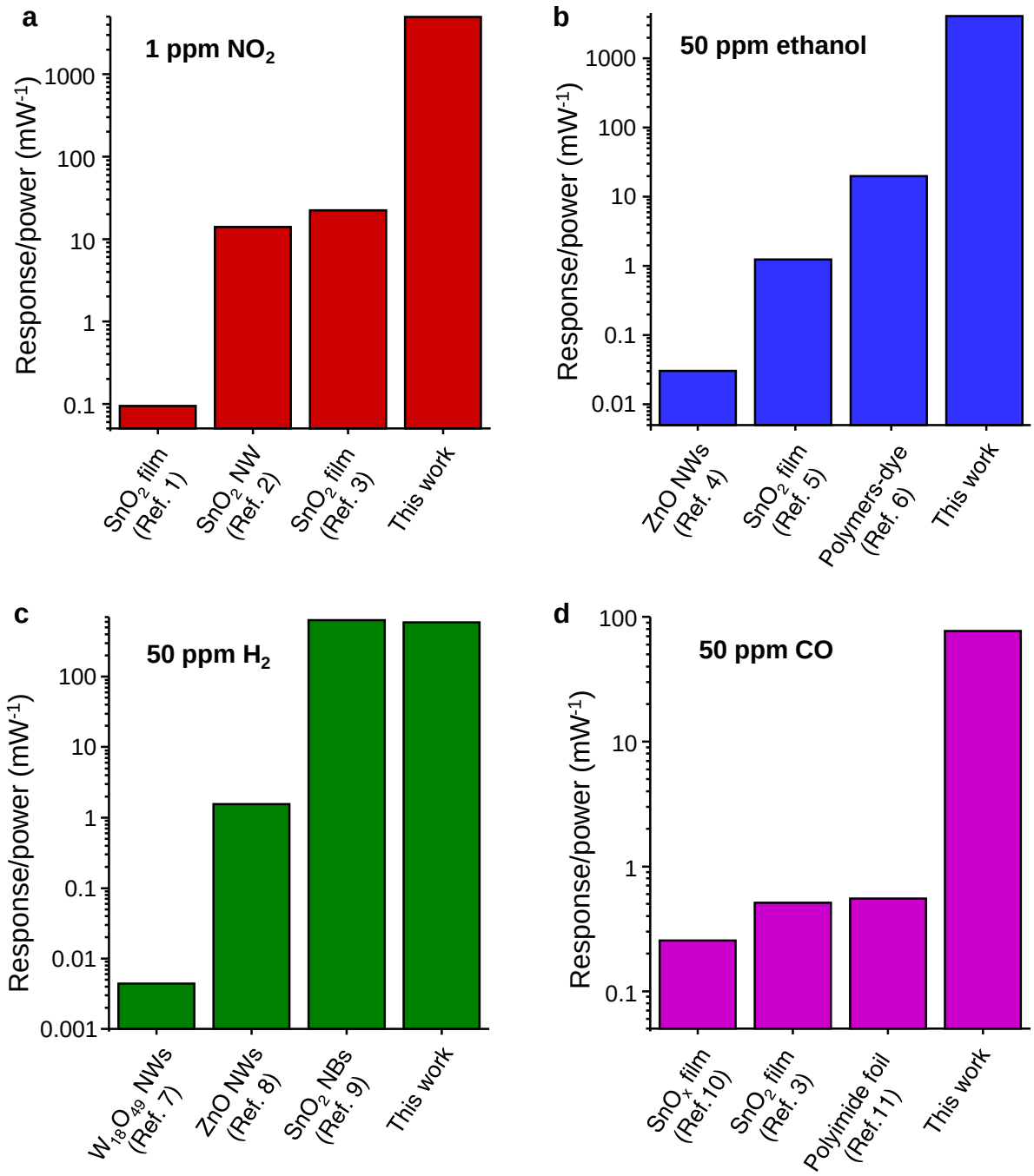

Supplementary Figure S10 | Comparison of figure of merit for our sensor with state-of-art chemoresistive sensors. a–d, Response/power values of previously reported high performance chemoresistive sensors[1–11] and our sensor to 1 ppm NO_2 (a), 50 ppm ethanol, 50 ppm H_2, and 50 ppm CO.

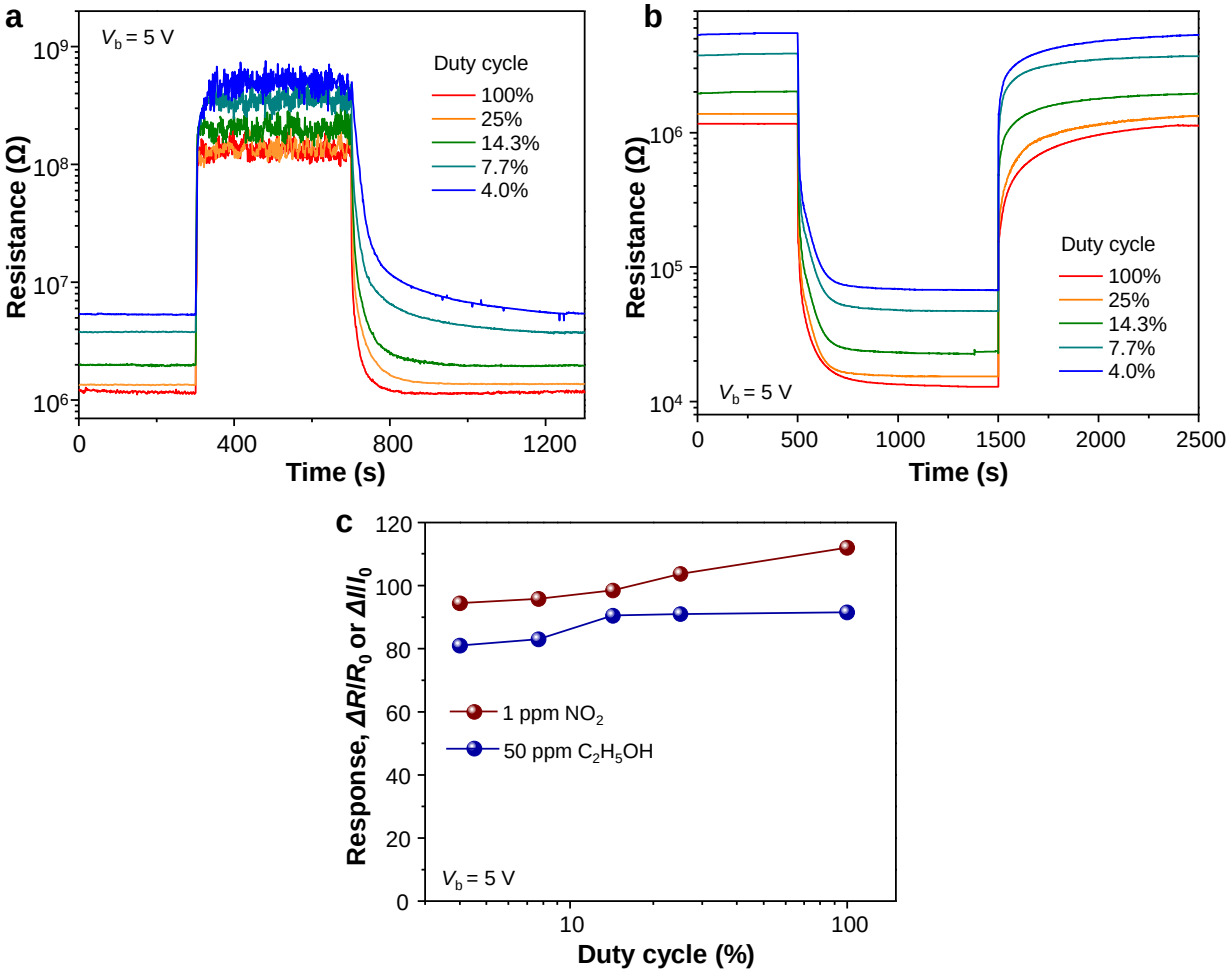

Supplementary Figure S11 | Dependence of sensor response and power consumption on the duty cycle of pulsed bias voltage. a,b, Sensing transients of a nanocolumnar WO_3 thin film sensor with 100 μm × 170 μm sensing area to 1 ppm NO_2 (**a**) and 50 ppm ethanol (**b**). The applied bias voltage to the sensors was 5 V. **c,** Response of the nanocolumnar WO_3 thin film sensor to 1 ppm NO_2 and 50 ppm C_2H_5OH as a function of sensing area.

1. Horrillo, M. C. et al. Detection of low NO_2 concentrations with low power micromachined tin oxide gas sensors. *Sens. Actuators B* **58**, 325–329 (1999).
2. Prades, J. D. et al. Ultralow power consumption gas sensors based on self-heated individual nanowires. *Appl. Phys. Lett*. **93**, 123110 (2008).
3. Elmi, I. Zampolli, S. Cozzani, E. Mancarella, F. Cardinali, G.C. Development of ultra-low-power consumption MO_X sensors with ppb-level VOC detection capabilities for emerging applications. *Sens. Actuators B* **135**, 342–351 (2008).
4. Santra, S. et al. ZnO nanowires grown on SOI CMOS substrate for ethanol sensing. *Sens. Actuators B* **146**, 559–565 (2010).
5. Llobet, E. et al. Screen-printed nanoparticle tin oxide films for high-yield sensor microsystems, *Sens. Actuators B* **96**, 94–104 (2003).
6. dos Reis, M. A. L. Thomazi, F. Nero, J. D. Roman, L. S. Development of a chemiresistor sensor based on polymers-dye blend for detection of ethanol vapor. *Sensors* **10**, 2812–2820 (2010).
7. Zhu, L. F. et al. Self-heated hydrogen gas sensors based on Pt-coated $W_{18}O_{49}$ nanowire networks with high sensitivity, good selectivity and low power consumption, *Sens. Actuators B* **153**, 354–360 (2011).
8. Ali, S. Z. et al. Nanowire hydrogen gas sensor employing CMOS micro-hotplate. *2009 IEEE Sensors* **1–3**, 114–117 (2009).
9. Strelcov, E. et al. Evidence of the self-heating effect on surface reactivity and gas sensing of metal oxide nanowire chemiresistors. *Nanotechnology* **19**, 355502 (2008).
10. Chan, P. C. H. et al. An integrated gas sensor technology using surface micro-machining. *Sens. Actuators B* **82**, 277–283 (2002).
11. Courbat, J. Briand, D. Yue, L. Raible, S. de Rooij, N. F. Drop-coated metal-oxide gas sensor on polyimide foil with reduced power consumption for wireless applications, *Sens. Actuators B* **161**, 862–868 (2012).